TOHEL 76-1
FERMILAB-PUB-76-133-E
E-83

Structure of dissociative clusters

T. Kitagaki, S. Tanaka, H. Yuta, K. Abe,
K. Hasegawa, A. Yamaguchi, T. Nozaki, K. Tamai,
R. Kikuchi, T. Maruyama and Y. Unno

Bubble Chamber Physics Laboratory
Tohoku University
Sendai, Japan

October 10, 1976

Separation of two clusters

We have measured approximately 11,000 pictures of the Fermilab 15' hydrogen bubble chamber exposed to 100 GeV π^- beam. In this paper the separation of dissociative clusters and the multiplicity distribution in the clusters are discussed using approximately 2,000 inelastic events of 2p — 8p. Slow protons were identified by bubble density and KPT check, and the loss of protons in higher momentum region is estimated to be 20%. In the following analysis we call the events with identified proton as proton events and the other as neutron events.

Fig.1(a) shows the rapidity distributions of pions and protons in CM in 4-prong proton events. The sharp peak seen in left side is proton peak and the hatched and black areas correspond to 4-prong 4C events. The figure shows two bumps in both sides of $Y > 0$ and $Y < 0$, i.e., the existence of group structure in each side of projectile and target. Therefore, we divide final state charged particles into two groups, forward and backward, where forward and backward are separated at the maximum rapidity gap in each event. In the following the notation $(n_p, n_t)_{\Delta Q}$ is used to assign a two cluster configuration, where n_p and n_t are the number of charged particles in the projectile and target clusters and ΔQ is the charge transfer from the target side to the projectile side.

Figs. 1(b) and (c) show the results of the separation of the 4-prong events into two configurations of $(1,3)_0$ and $(3,1)_0$, where proton peaks of 4p-4C are not shown. Both figures show the separation of two clusters in rapidity distribution becomes very clear by distincting each cluster configurations. 85% of events are picked up in these $(1,3)_0$ and $(3,1)_0$ configurations. The remainder of events are classified to $(2,2)_{-1}$, $(2,2)_{+1}$ and $(1,3)_{+2}$.

Table I

4-prong.	$(1,3)_0$	54%
	$(3,1)_0$	31
	$(2,2)_{-1}$	4
	$(2,2)_{+1}$	9
	$(1,3)_{+2}$	1

The separation of two clusters in forward and backward by the maximum rapidity gap is applied for all of 2p — 8p. Figs.2(a) - (d) show the distributions of rapidity gap length of the maximum gap and of the second maximum gap in each

topology. The distinction of the maximum gap length from the second maximum gap length is statistically meaningful up to 8-prong. Figs. 2(e) - (h) show the rapidities of the left end; and the right end points, Y_L and Y_R, of the maximum gaps. The sharp peak seen in Y_L is due to the existence of target side clusters at $Y < -2$ and the bump of Y_R is due to the projectile clusters in Y_R. They show the usefulness of the cut at the maximum rapidity gap.

As seen in the example of 4p, $\Delta Q = 0$ configurations are dominant in each event topology. Therefore, the purity of $\Delta Q = 0$ configuration obtained by the maximum rapidity gap method is not bad, however the signal to noise ratio in $\Delta Q \neq 0$ configurations should be carefully examined. The events classified in $\Delta Q \neq 0$ configuration could include (a) real even-even configuration, (b) a tail from the dominant $\Delta Q = 0$ configuration crosses over and (c) events inappropriate to classify into two cluster configuration.

Fig. 3A shows (a) $M(p\pi^+\pi^-)$ and (b) $M(p\pi^+)$ and (c) $M(p\pi^-)$ in the three body clusters $p\pi\pi$ in the configuration $(1,3)_0$. It is seen that the three particle combinations of $p\pi^+\pi^-$ make a low mass cluster and $p\pi^\pm$ combinations in the clusters easily make Δ_{1236} (the left end two bins). Figures (b), (c) and (d) in Figs. 3B and 3C are $M(p\pi^+)$ in $(2,2)_{-1}$ configuration and $M(p\pi^-)$ in $(2,2)_{+1}$ in each topology.

Δ_{1236} peaks are also seen up to 8-prong. However, $M(p\pi^+\pi^-)$ made forcibly from $(2,2)_{-1}$ and $(2,2)_{+1}$, (a) in Figs. 3B and 3C, does not show a clear low mass enhancement as seen in Fig. 3A(a).

Possible contamination from low mass $p\pi\pi$ may be less than 20% in Figs. 3B (a) and 3C (a). It proves that most of $(2,2)_{\pm 1}$ configurations selected by the maximum rapidity gap method are real $\Delta Q = \pm 1$ exchange, probably A_2 exchange in this energy region of 100 GeV.

Figs. 4A and 4B show similar plots of dipion combination in the projectile clusters of $(2,2)_{-1}$ and of $(2,2)_{+1}$. The excess of $M(\pi^+\pi^-)$ compared to $M(\pi^-\pi^-)$ shows ρ^o production. It is also shown that these ρ^o's do not come through three pion clusters as seen in Fig. 7A (b).

Effects of neutral particles

Figs. 5(b) and (c) are distributions of apparent missing masses MM_p and MM_t in the 4-prong proton events. The scatter plot (a) is superposed for two configuration of $(3,1)_0$ and $(1,3)_0$. Black areas in the missing mass spectra are derived from measured values of 4C events fitted by SQUAW. They concentrate sharply around $MM_p = MM_t = 0$ and show our experimental resolutions in the missing mass in both sides.

It is seen that two missing mass spectra in one side have similarity in spite of quite different configurations of charged particles and the general feature of spectrum shape in both

sides are different beyond the difference of resolutions. That is MM_t has a bump structure in high mass region, $M^2 > 50$, in contrast with a smooth short tail of MM_p. The feature is attributed to the dominant population of neutral mesons in projectile side compared to target side in $\pi^- p$ interactions.

Fig. 5 (d) is the longitudinal momentum of missing mass MM_n in CM for both of $(3,1)_0$ and $(1,3)_0$, where 4C events are removed. MM_n is the missing mass of all neutrals calculated from all charged particles. Fig. 5(d) clearly shows forward production of neutrals in projectile side. The hatched areas of Figs. 5 (c) and (b) are respectively:

$$5(c) \quad : MM_t \text{ for } P^*(MM_n) > 1.0 \text{ GeV},$$
$$5(b) \quad : MM_p \text{ for } P^*(MM_n) < -1.0 \text{ GeV}.$$

It proves that the high mass bump of MM_t is due to the forced combination of neutrals in projectile side and target side particles. Since neutrals are less populated in target side clusters, MM_p seen from target side is slightly deformed from the real mass of projectile cluster.

Results

The separation into two clusters are performed from 2-prong to 8-prong from the view point of the peripheral model, where the cluster includes single leading particle.

Fig. 6 shows the charged multiplicity distributions (a) in projectile cluster and (b) in target cluster for each event topology summed for all ΔQ. It is seen that the odd multiplicity is dominant in both clusters. Fig. 6(c) and (d) are similar multiplicity plots for each ΔQ value summed for event topologies. $Q = 0$ states are dominant.

However, non zero production of $\Delta Q = \pm 1$ states suggests the existence of $\Delta I = 1$ exchange with the order of 10% in these low mass region of clusters conventionally treated as the diffractive peak.

Figs. 7A shows the missing mass MM_p up to 8p for $\Delta Q = 0$ proton events with the condition;

(1) $(p\ell(\pi^+\pi^-))^+ X^-$ is derived from $((n - 2\ell + 1), (2\ell + 1))_0$ configurations, where ℓ is the number of $\pi^+\pi^-$ pair, with $\ell = 0$, 1, 2, 3.

Black area is with an additional condition;

(2) $P^*_{\parallel}(MM_n) > 0$.

The condition (1) reduces fake combinations due to charged particles and the condition (2) reduces the spurious combinations due to neutral particles.

The black areas show realistic mass distribution of dissociative clusters, since the distribution is much broader than the experimental resolution of the order of ± 2 $(GeV)^2$. They have sharp peaks near 0 and long tails of low level up to 100 $(GeV)^2$. The peak disappears from low mass side in general as the particle number increases.

Figs. 7B and 7C are the similar missing mass distributions of MM_t in proton events and neutron events with the conditions;

(1) $X^+(\pi^-\ell(\pi^+\pi^-))$ is derived from $((2\ell + 1), (n - 2\ell - 1))$ configurations, where $\ell = 0, 1, 2,$

(2) $P^*_{\parallel}(MM_n) > 0,$ for black area in Fig. 7B.

The peak near 0 is broader than that in the case of MM_t by the resolution.

Fig. 8 shows the charged multiplicity distributions of pion clusters, proton clusters, single diffractive events and total events. The Events following our definition of the diffractive dissociation, $\Delta Q = 0$, correspond to those black areas in Fig. 7. The clear in crease of the cross section difference from the conventional mass cut method is seen in the high multiplicity part.

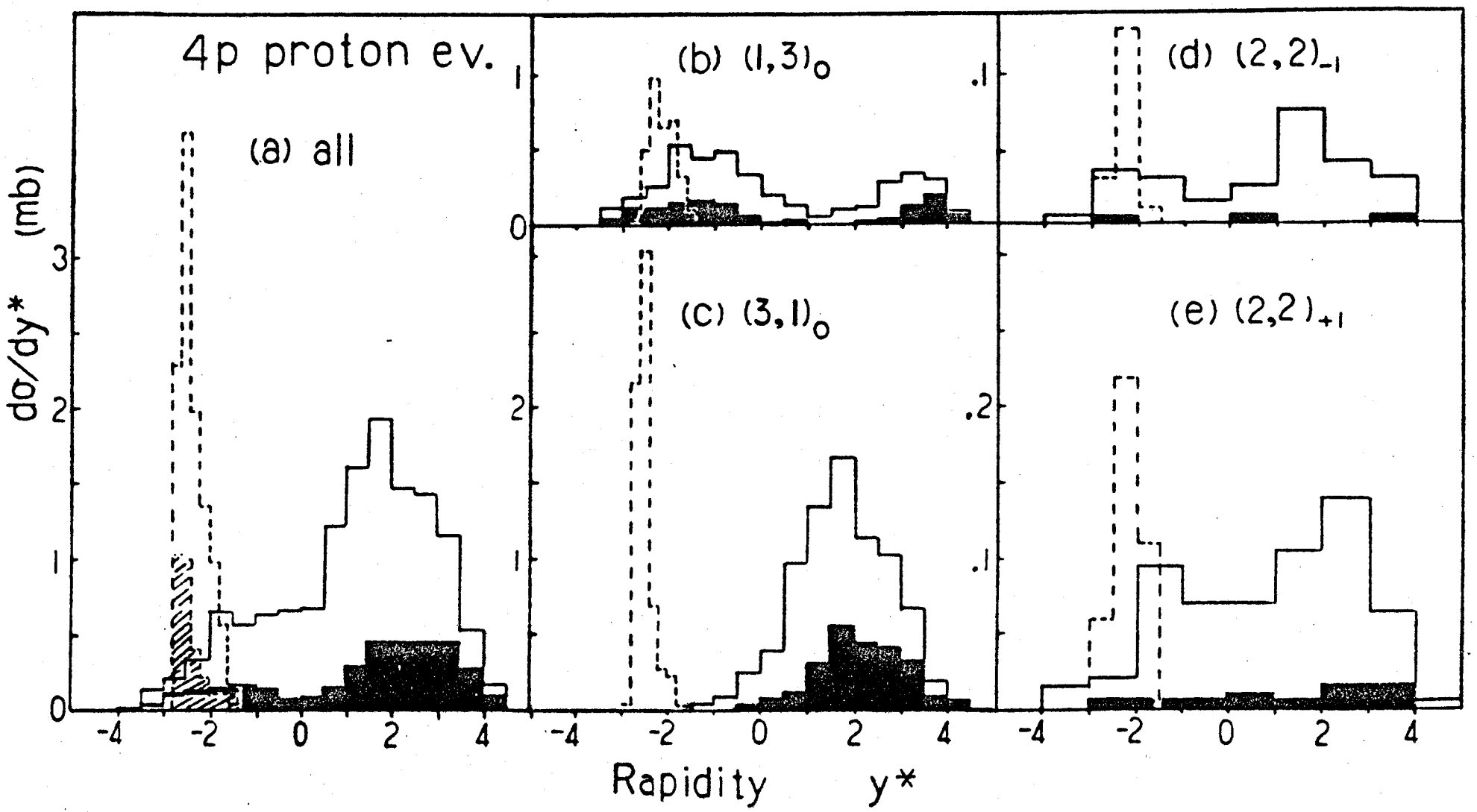

Fig. 1

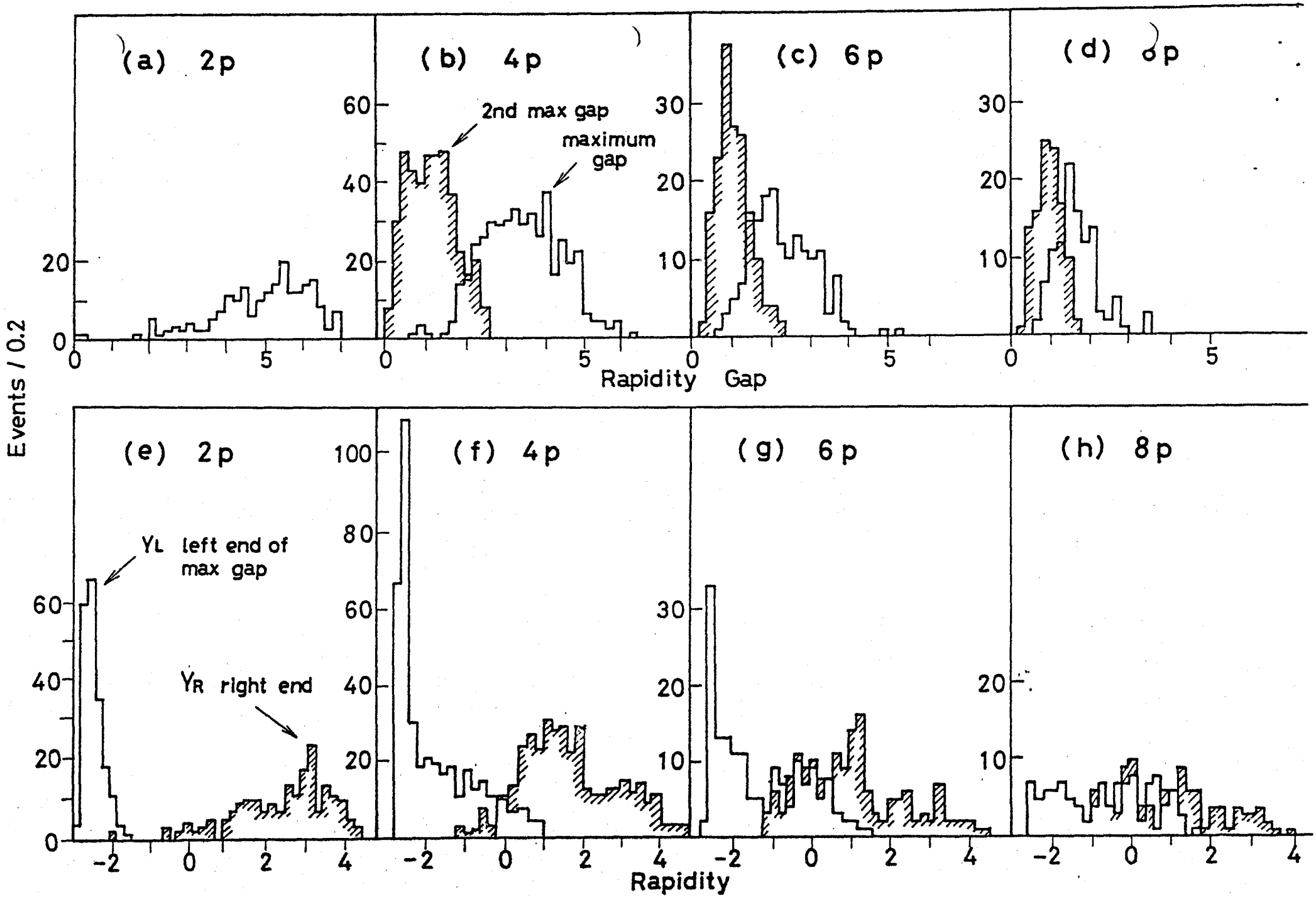
(a) 2p
(b) 4p
(c) 6p
(d) 8p
2nd max gap
maximum gap
Events / 0.2
Rapidity Gap
(e) 2p
(f) 4p
(g) 6p
(h) 8p
YL left end of max gap
YR right end
Rapidity

Fig. 2

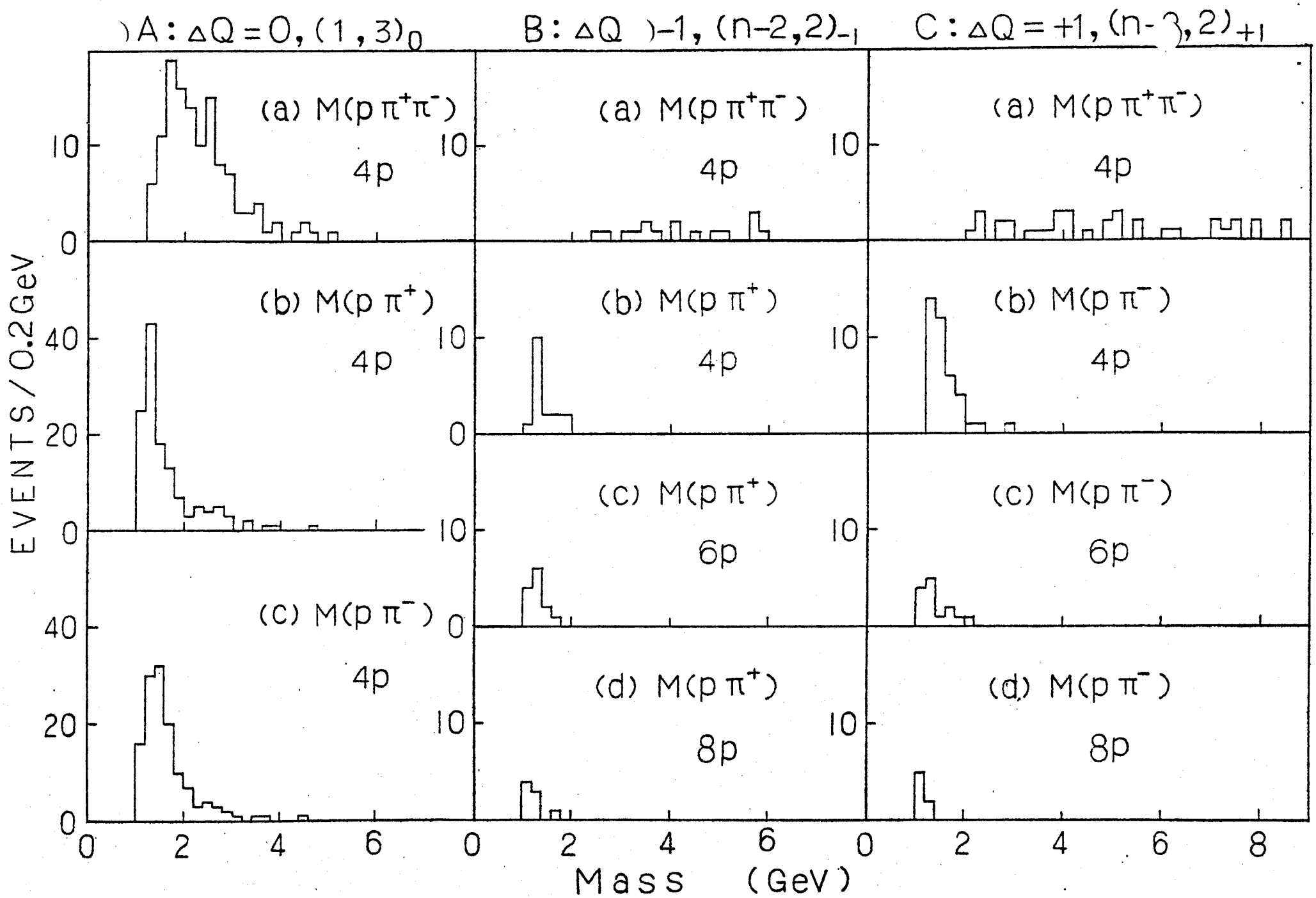
A: ΔQ = 0, (1, 3)0
B: ΔQ = −1, (n−2, 2)−1
C: ΔQ = +1, (n−3, 2)+1
(a) M(pπ+π−)
4p
(b) M(pπ+)
4p
(c) M(pπ−)
4p
(a) M(pπ+π−)
4p
(b) M(pπ+)
4p
(c) M(pπ+)
6p
(d) M(pπ+)
8p
(a) M(pπ+π−)
4p
(b) M(pπ−)
4p
(c) M(pπ−)
6p
(d) M(pπ−)
8p
EVENTS / 0.2GeV
Mass (GeV)

Fig. 3

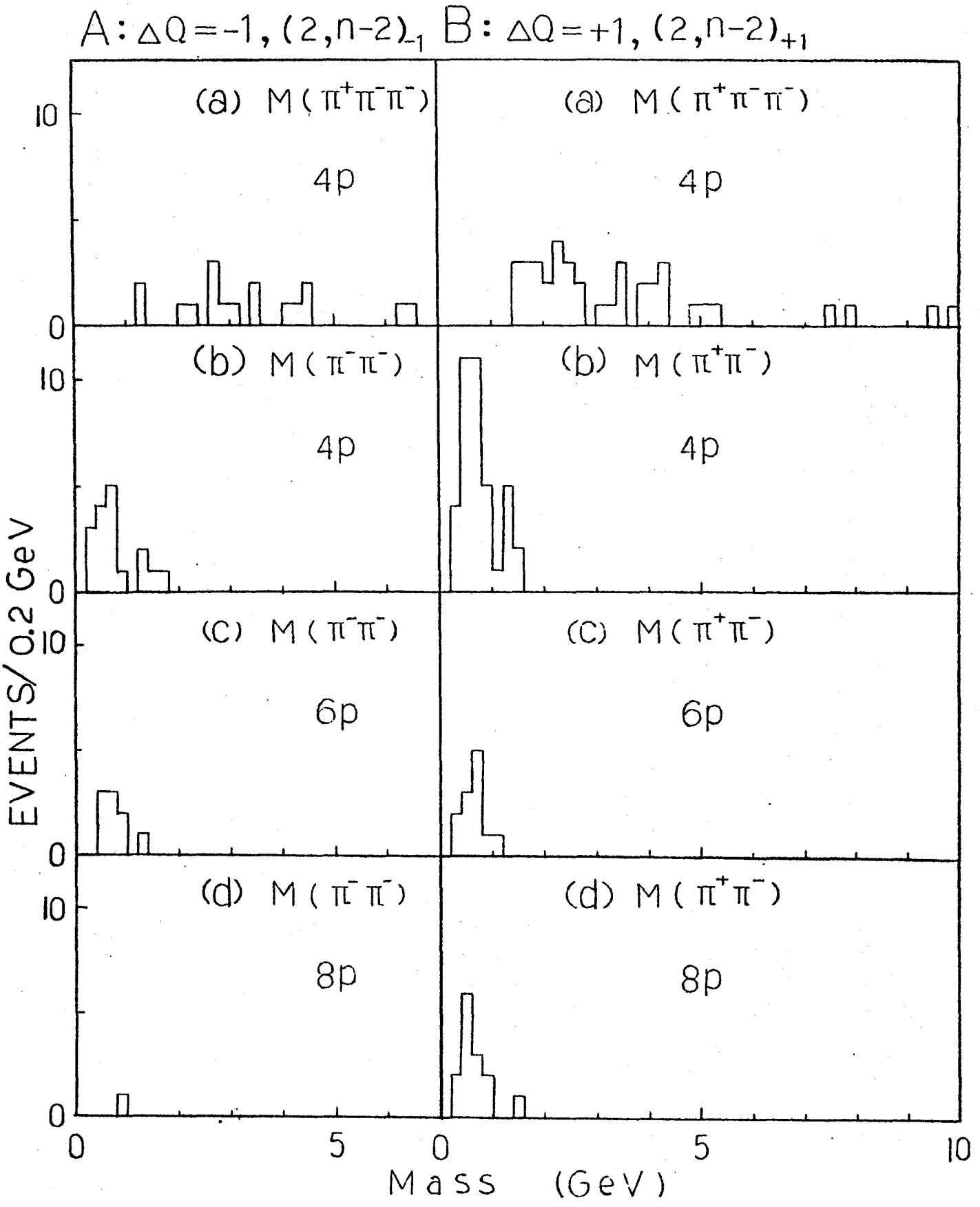
A: ΔQ=-1, (2,n-2)-1
B: ΔQ=+1, (2,n-2)+1
(a) M(π+π-π-)
4p
(b) M(π-π-)
4p
(c) M(π-π-)
6p
(d) M(π-π-)
8p
(a) M(π+π-π-)
4p
(b) M(π+π-)
4p
(c) M(π+π-)
6p
(d) M(π+π-)
8p
EVENTS/0.2 GeV
Mass (GeV)
0
5
10

Fig. 4

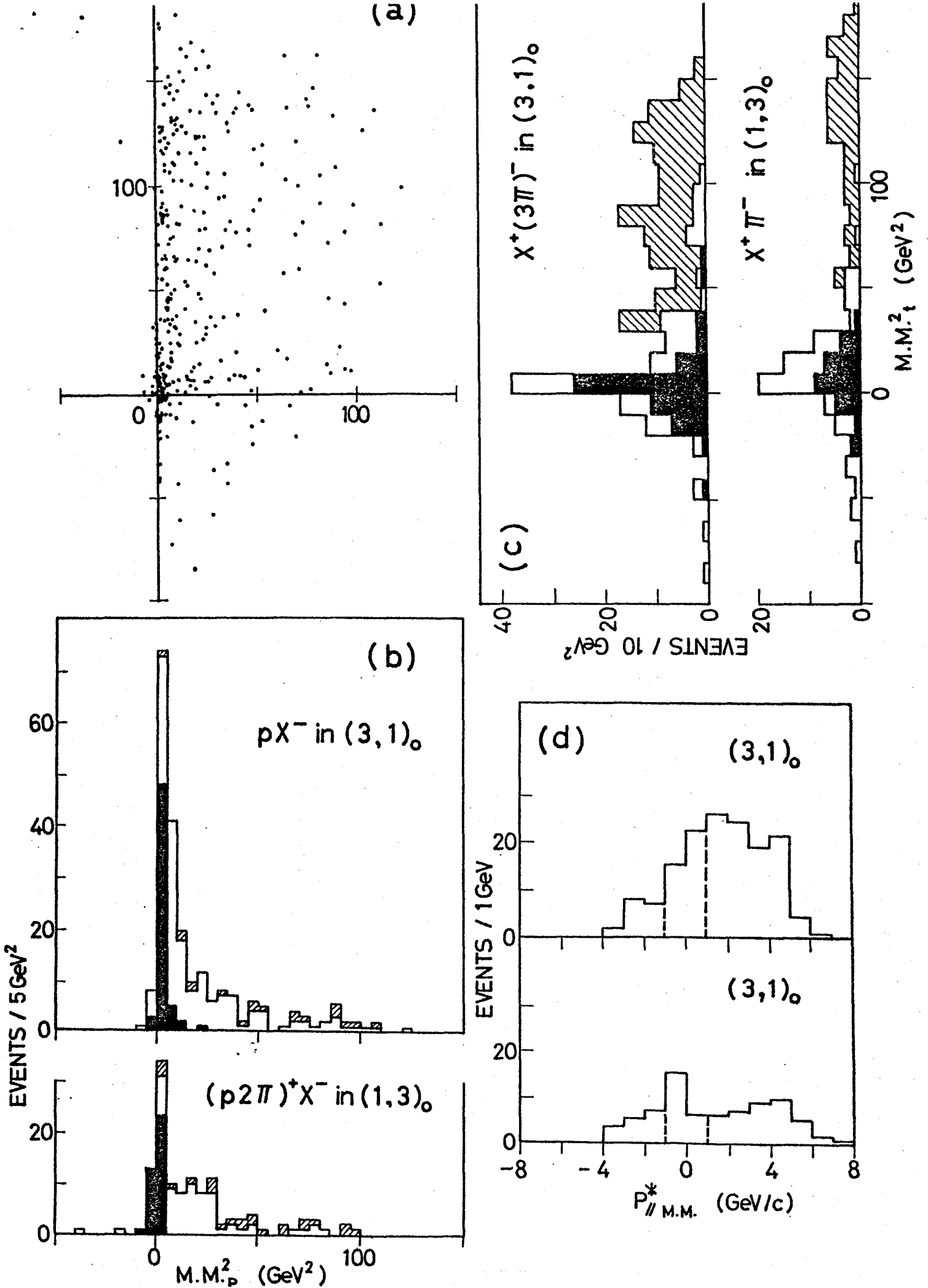
(a)
100
0
100
(b)
pX⁻ in (3,1)₀
(p2π)⁺X⁻ in (1,3)₀
EVENTS / 5 GeV²
60
40
20
0
20
0
0
100
M.M.²p (GeV²)
(c)
X⁺(3π)⁻ in (3,1)₀
X⁺π⁻ in (1,3)₀
EVENTS / 10 GeV²
40
20
0
20
0
0
100
M.M.²t (GeV²)
(d)
(3,1)₀
(3,1)₀
EVENTS / 1 GeV
20
0
20
0
-8
-4
0
4
8
P*// M.M. (GeV/c)

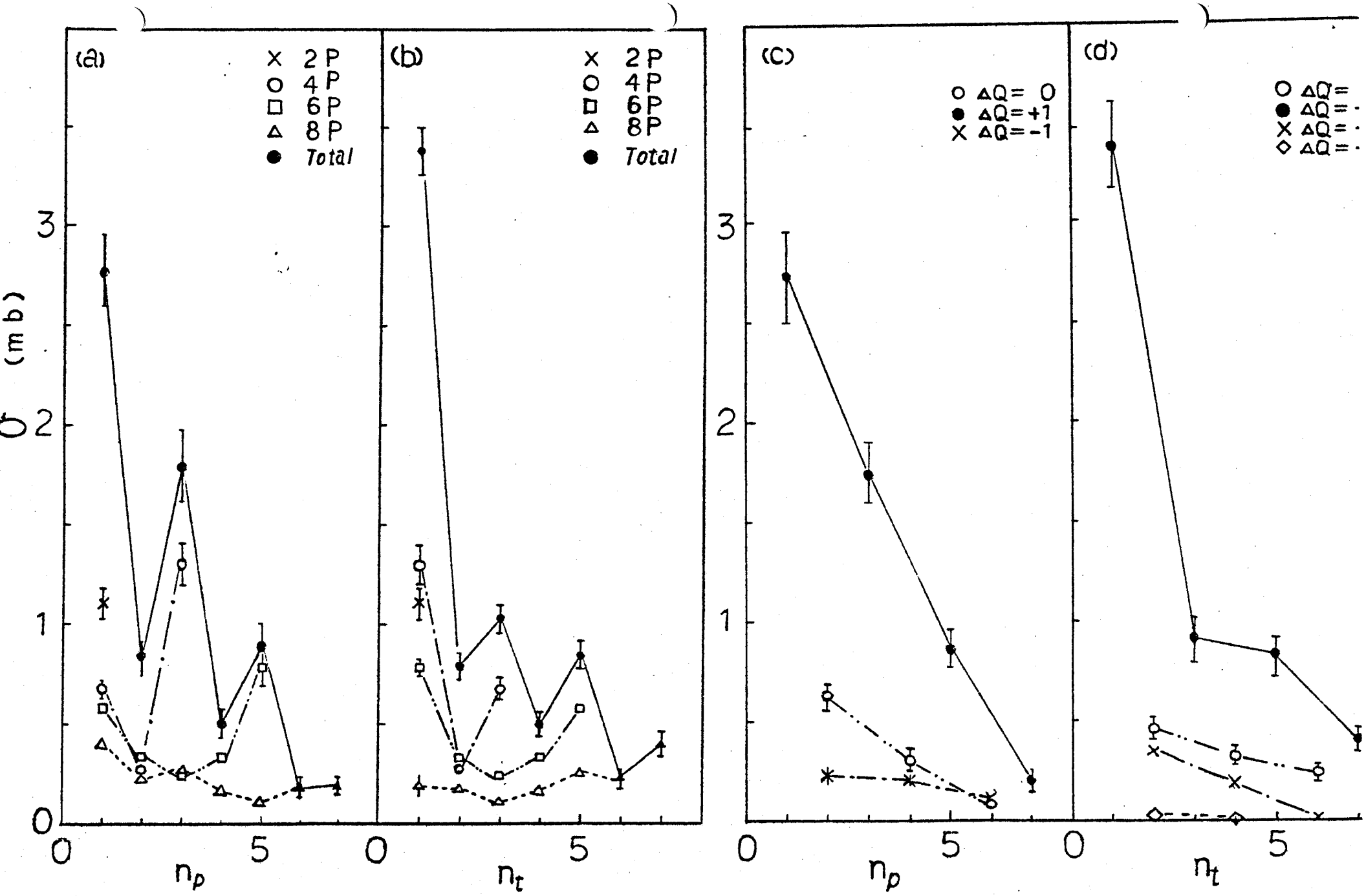
(a)
× 2P
○ 4P
□ 6P
△ 8P
● Total
(b)
× 2P
○ 4P
□ 6P
△ 8P
● Total
(c)
○ ΔQ= 0
● ΔQ=+1
× ΔQ=-1
(d)
σ (mb)
0
1
2
3
0
5
n_p
n_t

Fig. 6

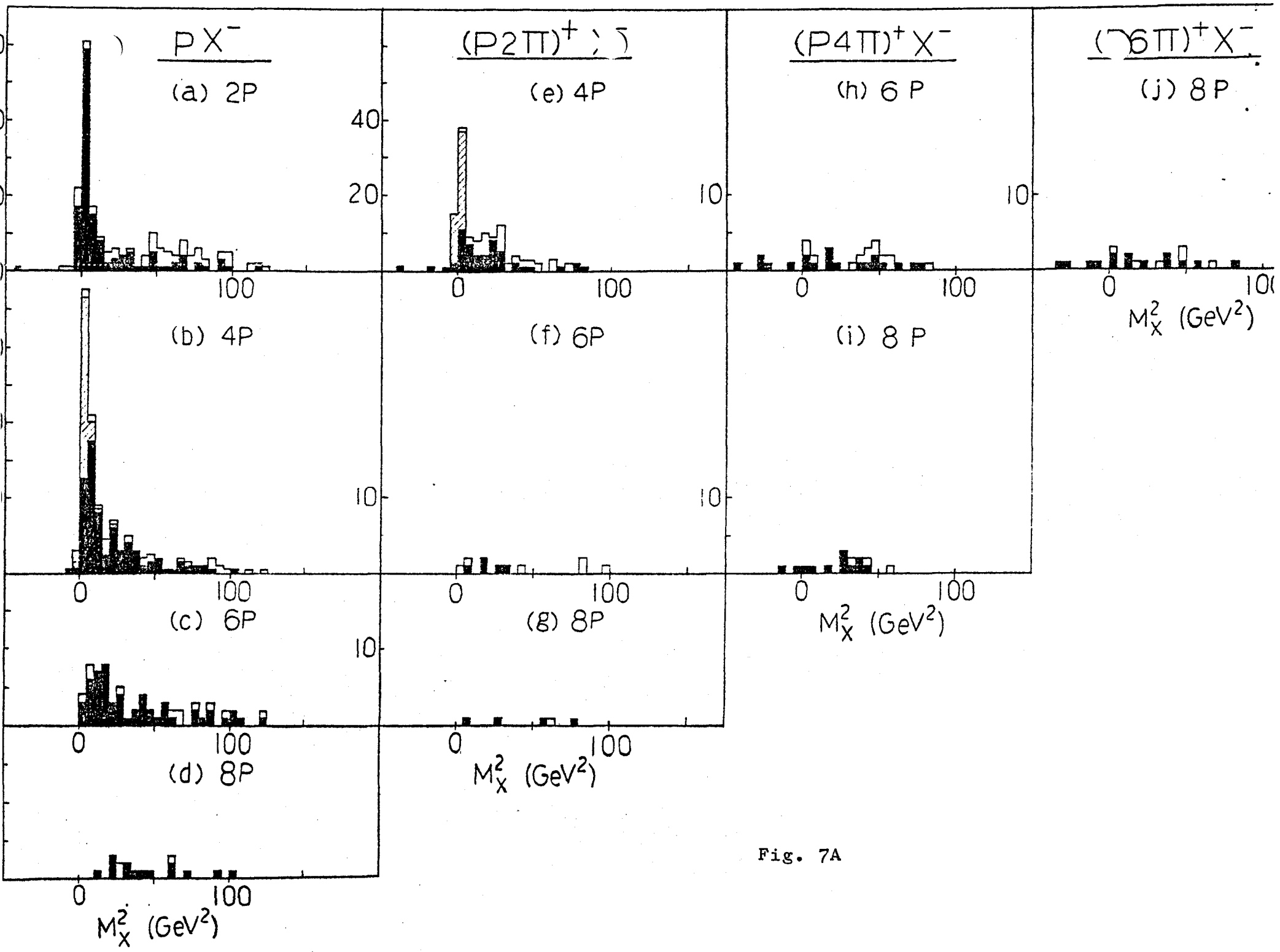
PX⁻
(a) 2P
(b) 4P
(c) 6P
(d) 8P
(P2π)⁺X⁻
(e) 4P
(f) 6P
(g) 8P
(P4π)⁺X⁻
(h) 6 P
(i) 8 P
(P6π)⁺X⁻
(j) 8 P
40
20
10
0
100
M²X (GeV²)

Fig. 7A

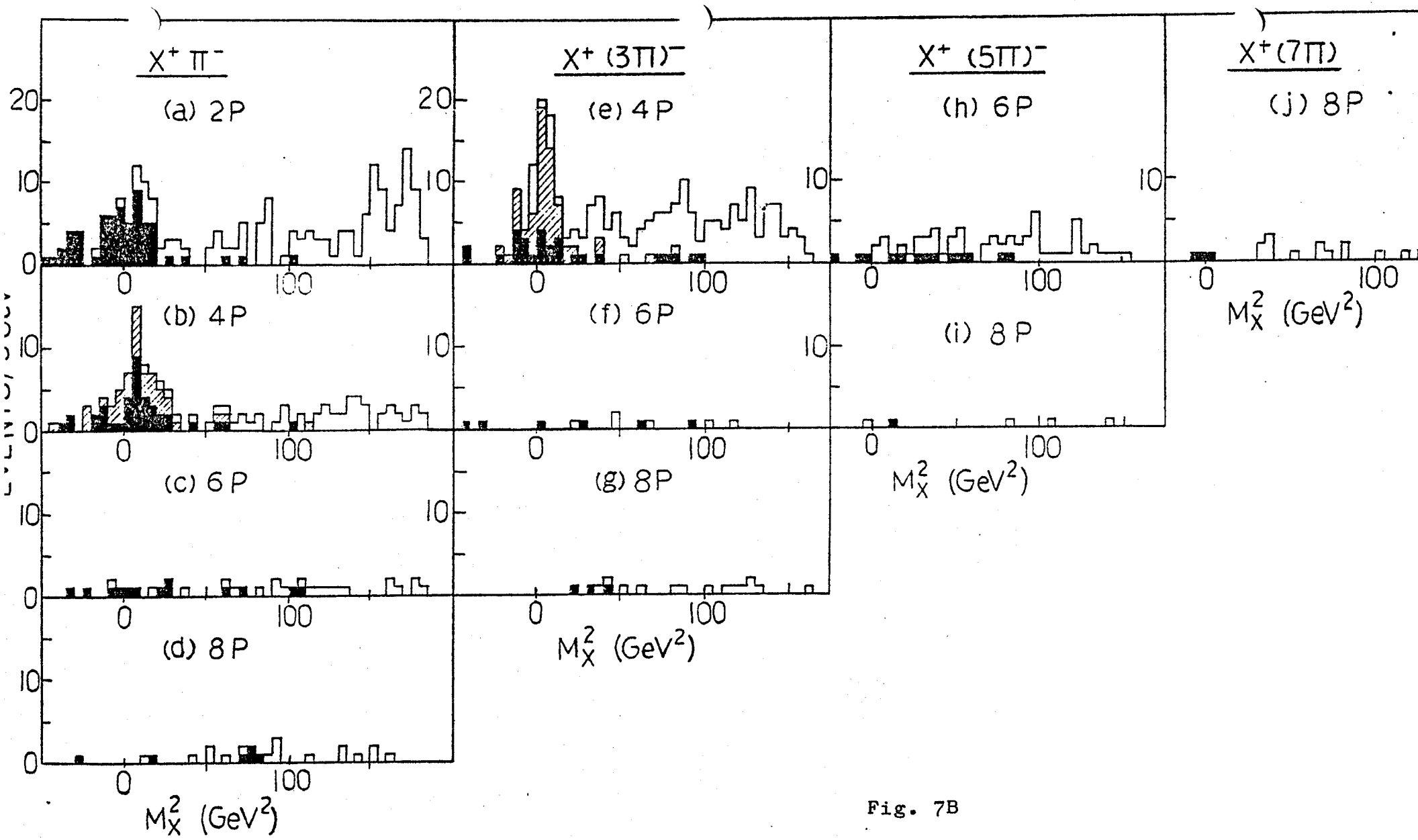
X+ π−
(a) 2P
(b) 4P
(c) 6P
(d) 8P
X+ (3π)−
(e) 4P
(f) 6P
(g) 8P
X+ (5π)−
(h) 6P
(i) 8P
X+(7π)
(j) 8P
20
10
0
100
M²X (GeV²)

Fig. 7B

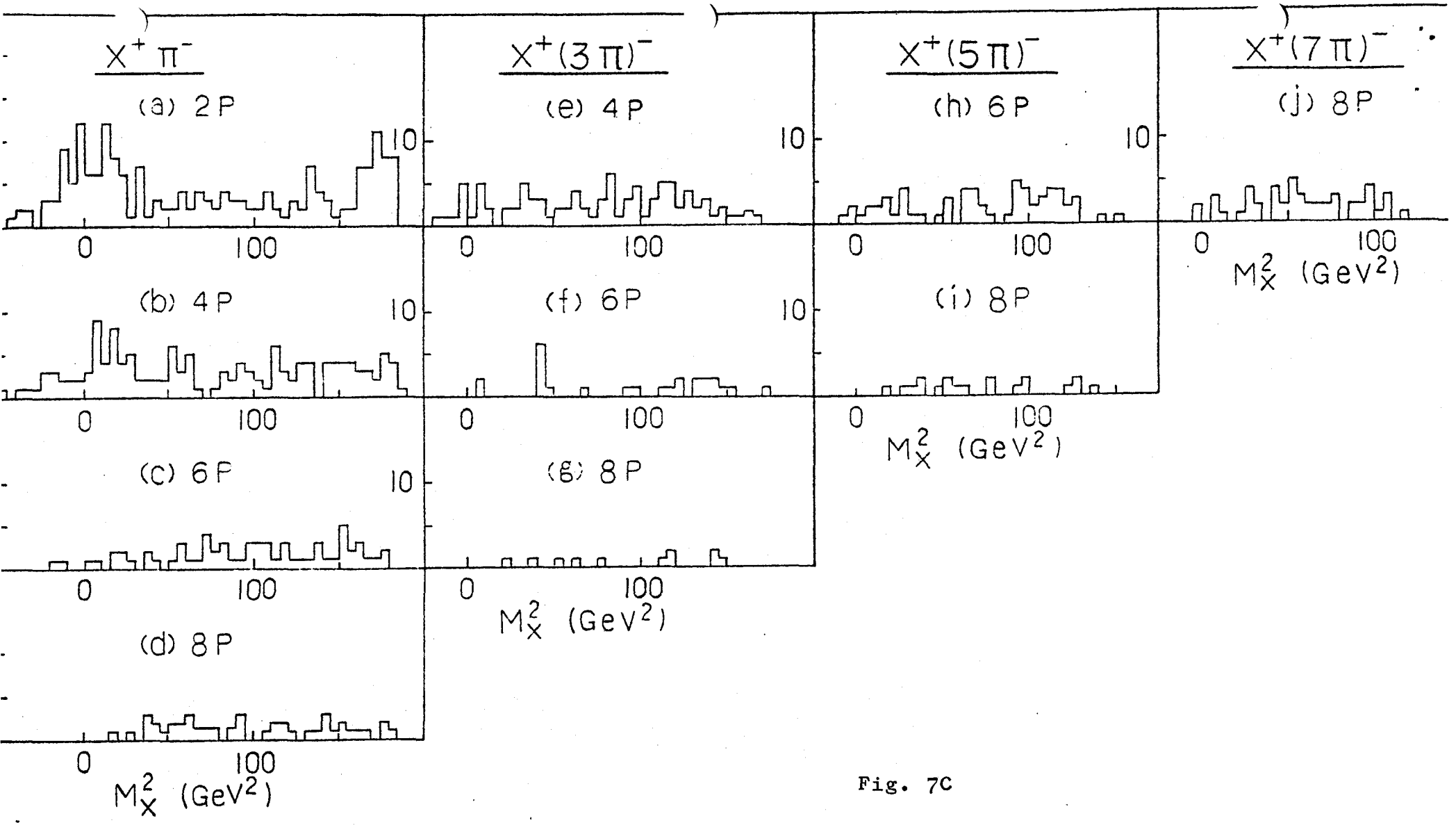
X+ π−
(a) 2P
(b) 4P
(c) 6P
(d) 8P
X+(3π)−
(e) 4P
(f) 6P
(g) 8P
X+(5π)−
(h) 6P
(i) 8P
X+(7π)−
(j) 8P
10
0
100
M²X (GeV²)

Fig. 7C

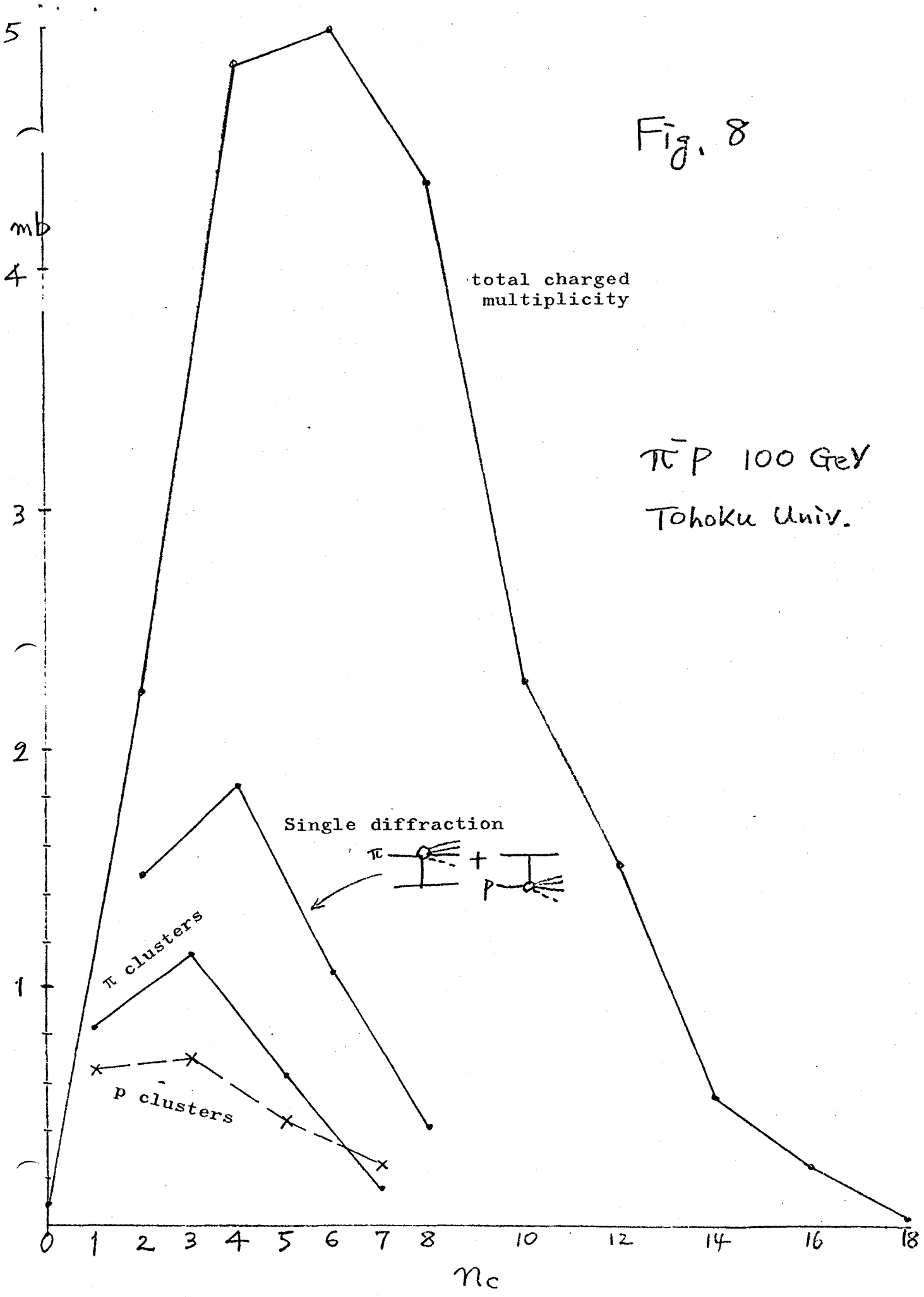
Fig. 8
mb
5
4
3
2
1
total charged multiplicity
$\pi^- p$ 100 GeV
Tohoku Univ.
Single diffraction
π
p
π clusters
p clusters
0 1 2 3 4 5 6 7 8 10 12 14 16 18
n_c